STUDIES ON THE OPTIMUM PERFORMANCE OF TAPERED VORTEX FLAPS

Kenichi RINOIE
Department of Aeronautics and Astronautics,
University of Tokyo, Tokyo, 113-8656, JAPAN

Keywords: *vortex flap, leading-edge separation vortex, delta wing*

Abstract

The effects of sweepback angles, leading-edge shapes and flap hinge-line positions over the performance of the leading-edge vortex flaps are discussed in this paper. As the sweepback angle decreases, improvements of the lift/drag ratio are attained over a wider lift coefficient range when compared with a slender delta wing. A rounded leading-edge vortex flap improves the lift/drag ratio at a relatively higher lift coefficient for both the 50° and 60° delta wings. The differences of the vortex flap hinge-line position also affect the performance of the vortex flap. The best lift/drag ratio is attained when the delta wing has vortex flaps with a relatively small spanwise length.

1 Introduction

The leading-edge vortex flap is a full span deflectable surface at the leading-edge of a delta wing [1]. With the flap deflected downward, a leading-edge separation vortex is formed over the forward facing flap surface. The suction force generated by the vortex acts on the flap and generates a thrust component (Fig.1 a, b). Hence it reduces the drag and improves the lift/drag (*L/D*) ratio, an essential factor for the improvement of the take-off and climb performance of the delta wing aircraft. Many studies have confirmed the benefit of the vortex flap [2-4].

There are three factors that mainly affect the vortex flap characteristics: firstly sweepback angles, secondly, leading-edge shapes i.e. sharp or rounded leading-edge and thirdly flap hinge-line positions. The author has made experimental studies using delta wing models that have sweepback angles Λ of 50°, 60° and 70°, fitted with tapered vortex flaps [5-7]. Throughout these studies, the benefit of the vortex flap was confirmed and the effect of the sweepback angle was revealed.

The author also conducted wind tunnel studies to know the effect of the second factor, i.e. the difference between sharp and rounded leading-edge vortex flaps [8] (Fig. 1 c, d). It was shown that deflecting the rounded leading-edge vortex flaps improves the *L/D* at relatively higher lift coefficients when compared with the sharp edged vortex flaps.

This paper mainly investigates the third factor, the effect of the vortex flap hinge-line positions (i.e. spanwise length of the vortex flap). The relationship between the spanwise length of the leading-edge separation vortex and that of the vortex flap may play an important role for the performance of the vortex flap. Therefore, wind tunnel tests using 60° delta wing models with four different flap hinge-line positions were conducted.

Figure 2 shows a schematic diagram of a delta wing with tapered vortex flaps used for the wind tunnel studies. The delta wing has vortex flap hinge-lines running from the wing apex to the trailing-edge. The vortex flap deflection angle δ_f is defined as the angle measured in the plane normal to the hinge-line. The flap hinge-line position *fr* is defined as:

$$fr = h / (b/2) ,$$

where *h* is the length between the flap hinge-line and the wing center line at the trailing-edge and *b*/2 is the semispan length at the trailing-edge. As for the plain delta wing without vortex flaps, *fr* equals to 1.

The vortex flap experiments conducted by the present author are summarized in Table 1. Preliminary experiments are also included in

this table [9,10]. Details of the experiments are shown in each reference. Experimental details whose data are discussed in this paper are described in the following sections. Except noted, most of the experiments were made at *fr*=0.75 and with sharp leading-edges.

In this paper, the effects of the sweepback angles and leading-edge shapes are briefly discussed. Then the discussion of the effect of the flap hinge-line position is made. The aim of this paper is to discuss the optimum vortex flap configurations that can attain the maximum performance, by examining the measured results of delta wings that have different sweepback angles, different leading-edge shapes and different flap hinge-line positions.

2 Effect of Sweepback Angle

2.1 Benefit of a Vortex Flap on *L/D*

Figure 3 shows the *L/D* - C_L distributions for the wing with and without flap deflection on the 50°, 60° and 70° delta wings [5-7]. These figures show that the greatest percentage improvement in the *L/D* ratio for δ_f =30° is about 40% at a C_L of 0.45 for the 60° delta wing and is about 26% at a C_L of 0.2 for the 70° delta wing. Figure 3 confirms the benefit of the vortex flaps.

A large *L/D* improvement for δ_f =20° of 50° delta wing is seen over the C_L range of 0.15 to 0.7 in Figure 3a. Figure 3b shows that the *L/D* of the 60° delta wing with δ_f =30° is greater than that of the δ_f =0° wing in the C_L range between 0.15 and 0.6. Figure 3c shows that the *L/D* benefit of the 70° delta wing with δ_f =30° is only seen in the C_L range between 0.1 and 0.25. The C_L range in which the *L/D* is improved for the 70° delta wing is much narrower than those for the 50° and 60° delta wings [7]. As the sweepback angle increases, the frontal area of the vortex flap decreases. This may have affected the *L/D* distributions for the 70° wing, a kind of a slender delta wing.

It was also revealed that the highest *L/D* for the 50° and 60° models is achieved using a modest flap deflection angle that causes a flow to attach to the flap surface without any large separation [5,7]. However, the maximum *L/D* for the 70° delta wing is attained, when a separated region is formed on the vortex flap and when the spanwise length of this separated region almost coincides with the vortex flap width [6]. This observation for the 70° delta wing agrees with the idea from the optimum vortex flap configurations, as proposed in Ref. 1.

2.2 Cross Flow Patterns

Figure 4 shows cross flow pattern sketches for the 60° and 70° delta wings plotted against the angle of attack α and the streamwise flap deflection angle δ_{fs}. These flow pattern sketches were deduced from the surface pressure measurements and from the oil-flow visualisation tests.

A streamwise flap deflection angle δ_{fs} is used as a parameter which controls the behaviour of the vortex flaps [11]. The δ_{fs} is derived by:

$$\delta_{fs} = \tan^{-1} (\sin \varepsilon \cdot \tan \delta_s) ,$$

where ε is a semi apex angle of the main wing alone, i.e. inboard the flap hinge-line (see Figure 2). The wing configuration $\delta_{fs} = \alpha$ means that the direction of the free stream coincides with the direction of the flap surface. When $\delta_{fs} < \alpha$, the stagnation point is expected to be located on a lower surface of the flap and a separation occurs on the upper surface. When $\delta_{fs} > \alpha$, the separation occurs on the lower surface. It is noted that the flow direction near the wing is not parallel to the direction of the free stream. Therefore, the above discussion is only a rough estimation. However, δ_{fs} may be used as a parameter representing the occurrence of separation on the flap surface.

Figure 5 summarizes the cross flow patterns obtained from Figure 4. The flow patterns around the vortex flap can be divided into 5 different areas:

A (low α, high δ_{fs}): Separation occurs on lower surfaces.

B (modest α, high δ_{fs}): Separation occurs inboard the flap hinge-lines.

C (low α, modest δ_{fs}): Although there is no separation around the flaps, C_L is very low and the friction drag C_{D0} is much larger than the vortex drag, hence the L/D is not improved.

D ($\alpha < \delta_{fs}$): As noted above, separation occurs on the upper surface.

E (modest α, modest δ_{fs}): The maximum L/D is attained in this area. As was also noted above, the sweepback angle decides whether the separation vortex is formed on the flap surface (Λ=70°), or no larger separation is formed (Λ=50°, 60°), when L/D attains its optimum for each wing.

3 Effect of Rounded Leading-edge

3.1 60° Delta Wing

In Reference 8, the effect of a rounded leading-edge on the 60° delta wing with vortex flaps has been investigated. Three different rounded edge diameter of D/Cr=0.5, 1.5 and 3% were tested, where Cr is a root chord length. The % increase in the L/D for the rounded leading-edge with and without flap deflection as compared with the sharp leading-edge flat delta wing (SLE/00) is plotted in Figure 6. In this figure, R15/30 denotes D/Cr=1.5% rounded edge wing with a flap deflection δ_f of 30°. Results of the sharp leading-edge wing when δ_f =30° (SLE/30) are also shown. This figure shows that the L/D without any flap deflection (R15/00 and R30/00) increases to more than 10% above that of the SLE/00 wing for lift coefficients greater than 0.2. The sharp edged vortex flap wing (SLE/30) shows better performance than R15/00 and R30/00 in the C_L range between 0.2 and 0.6. The most significant L/D improvement, which is more than 50% as compared with the sharp flat delta wing, is observed for R30/30 at about C_L=0.6.

3.2 50° Delta Wing

In order to know the effect of the rounded leading-edge in detail, further wind tunnel studies using the 50° delta wing model with vortex flaps have been made [12].

3.2.1 Experimental Details

Figure 7 shows the details of the model. The model is a 50° flat plate delta wing with no camber. The centre-line chord length Cr is 0.5m. The main wing inboard the flap hinge-lines is a flat plate and the thickness is 0.009m. The upper and lower surfaces of all edges are beveled. The rounded leading-edge radius is 4.5mm. The sharp leading-edge vortex flap was also tested. The sharp edged vortex flap outboard of the flap hinge-line is made of a 2mm flat thickness plate. Configurations of δ_f =0°, 10°, 20° and 30° were tested.

The experiments were made in the 2m diameter open test section of the Gottingen-type wind tunnel at the University of Tokyo. All the tests were done at a tunnel speed of U_∞ = 20m/s. The Reynolds number based on the wing centre line chord Re_{Cr} was 6.7×10^5. The model was suspended by wires from a three component balance. The lift, drag and pitching moment were measured using this balance. The wire tare drag effect was taken into account and the tunnel boundary corrections were applied to the measured data. The incidence α was increased from -5° to 20°. Because of the tunnel balance geometry, incidences greater than 20° could not be used. All aerodynamic coefficients were based on the same datum wing area (δ_f =0°). Flow visualisation tests using surface oil flow were conducted to describe the flow around the wing. The estimated overall accuracy of the aerodynamic coefficients is ±3% at 20:1 odds.

3.2.2 Experimental Results

Figures 8 shows the lift to drag ratio (L/D) versus C_L when δ_f =0° and 20°. Although both the sharp edge and rounded edge wings with δ_f =20° improve the L/D when compared to the sharp edge wing without flap deflection (SLE, δ_f =0°), it is seen that the sharp edged wing is more efficient in improving the L/D. However, at C_L values greater than 0.35, the rounded edge

wing with flap deflection show better *L/D* ratios than the SLE δ_f =20°. Although the sweepback angle of the delta wing is different, these results confirm the conclusion obtained for a 60° wing with a rounded leading-edge [8].

As noted in Ref. 8, the effects of the Reynolds number are dominant for the rounded leading-edge delta wing. Therefore, further studies with different Reynolds numbers are necessary to investigate the rounded edge vortex flap.

4 Effect of Flap Hinge-line Positions

4.1 Experimental Details

Figure 9 shows details of delta wing models. The 60° flat plate delta wing models with sharp leading-edges that have different flap hinge-line positions of *fr*=0.6, 0.75, 0.9 and 1.0 were used. The centre-line chord length *Cr* is 0.5m. The upper and lower surfaces of all the edges are beveled. Flap configurations of δ_f =30° were tested.

The same wind tunnel described in Section 3 was used for the tests. All tests were done at a tunnel speed of U_∞ = 20m/s. The Reynolds number based on the wing centre line chord Re_{Cr} was 6.7×10^5. Lift, drag and pitching moment were measured. All aerodynamic coefficients were based on the same datum flat plate delta wing area (*fr*=1.0). Flow visualisation tests using surface oil flow were also conducted.

4.2 Experimental Results

The C_L vs. α curves are shown in Figure 10 for various *fr*s. This figure shows that the C_L decreases as *fr* decreases, that is, as the vortex flap area increases. The C_D - α curves (Figure 11) show that the C_D decreases for most of the positive α region, as *fr* decreases. These trends in C_L and C_D are similar to those when δ_f is increased at constant *fr*.

Figure 12 shows the *L/D* versus C_L. A large *L/D* improvement for δ_f =30° is seen over the C_L range of 0.15 to 0.5. The maximum *L/D* is attained when *fr*=0.9. However, the benefit of *fr*=0.9 is only seen for the C_L range between 0.2 and 0.25. When C_L>0.25, fr=0.75 indicates the best performance. Although all of the configurations (*fr*=0.9, 0.75 and 0.6) show benefit in the *L/D* when compared with *fr*=1.0 wing (plain delta wing), it is seen that the *fr*=0.6 wing is the least effective. Ref. 13 reported the effect of flap hinge-line positions for a 60° delta wing when the *fr*=0.5 and 0.75. The results indicated that the *fr*=0.5 wing is less effective than the *fr*=0.75 wing.

Figure 13 shows the pitching moment curves measured around the model centre of the area *x/Cr*=0.67 for all tests. The tapered vortex flap has little effect on C_m as was also discussed in Refs. 5-7.

Figure 14 shows the surface flow patterns sketched from oil flow tests of the upper surface of the right wing at α =8°, 10° and 12° for *fr*=0.6 and 0.75. The patterns define the vortex positions on the wing and flap surfaces. In these figures, H.L. denotes the flap hinge-line. The hatched region denotes a small separation bubble, in which, the oil moved very little. At α =8° for both the *fr*=0.75 and 0.6 wings, there are only small separation bubbles (hatched regions) at the leading-edge of the flap and at the flap hinge-line. The flow attaches on the flap surface without any large separation. At α =10° for *fr*=0.75, a leading-edge separation vortex is formed. Near the apex, the vortex reattaches inboard of the flap hinge-line. Near the trailing-edge, the chordwise length of the vortex reduces and the vortex reattaches on the flap surface. At α =12° for *fr*=0.75, the reattachment of the vortex occurs inboard of the hinge-line for the whole chordwise stations. On the other hand, as for the *fr*=0.6 wing, the leading-edge separation vortex is constrained only over the flap surface at α =10° and 12°.

Figure 15 shows the cross flow patterns plotted against α and *fr*. Flow patterns are deduced from the surface oil flow tests. The wing configuration, when the *L/D* attains its local maximum for a constant *fr*, is shown by the symbol *. This figure shows that the cross flow patterns can be divided into 4 different patterns. First, the leading-edge separation

vortex is not formed and only a small separation bubble is formed at the leading-edge or at the flap hinge-lines (at low α, all *fr*). Second, the leading-edge separation vortex is formed only over the flap surface (at α =10°-16°, *fr*=0.6 only). Third, the large separation vortex is formed and its reattachment line is located inboard of the flap hinge-lines (at high α, all *fr*). Finally, there is a configuration where the reattachment of the vortex occurs on the flap surface near the wing apex, but the reattachment occurs inboard the flap hinge-line near the trailing-edge, as is seen in Figure 14 (at about α =10°, *fr*=0.75 and 0.9). This figure shows that the formation of a leading-edge separation vortex for the plain delta wing (*fr*=1) is seen at α > 3° for the first time when α is increased from 0°. However, once the flap is deflected, even though its spanwise length is only 10% (*fr*=0.9), the angle of attack when the vortex is formed for the first time is α =7°. This indicates that a large change of flow pattern occurs even when a vortex flap that has small spanwise length is deflected (*fr*=0.9). This may be related to the fact that the maximum *L/D* was attained for the fr=0.9 wing when C_L was relatively small, as was shown in Figure 12.

5 Conclusions

In this paper, the effects of sweepback angles, leading-edge shapes and flap hinge-line positions over the performance of the leading-edge vortex flaps have been discussed.

1) As the sweepback angle decreases, improvements of the lift/drag ratio are attained over a wider lift coefficient range when compared with a slender delta wing.

2) The rounded leading-edge vortex flaps improve the lift/drag ratio at a relatively higher lift coefficient for both the 50° and 60° delta wings.

3) Differences of the vortex flap hinge-line position affect the performance of the vortex flap. The best lift/drag ratio is attained when the delta wing has vortex flaps with a relatively small spanwise length.

Acknowledgements

The author would like to express his gratitude to Dr. D. Kwak, Mr. K. Yamagata and Mr. Y. Sunada for their help in conducting the wind tunnel experiments.

References

[1] Rao D M. Leading edge vortex-flap experiments on a 74deg. delta wing. NASA CR-159161, 1979.

[2] Marchman III J F. Effectiveness of leading-edge vortex flaps on 60 and 75 degree delta wings. *Journal of Aircraft*, Vol. 18, No. 4, pp 280-286, 1981.

[3] Frink N T. Subsonic wind-tunnel measurements of a slender wing-body configuration employing a vortex flap. NASA TM-89101, 1987.

[4] Traub L W. Aerodynamic characteristics of vortex flaps on a double-delta planform. *Journal of Aircraft*, Vol. 32, No. 2, pp 449-450, 1995.

[5] Rinoie K and Stollery J L. Experimental studies of vortex flaps and vortex plates. *Journal of Aircraft*, Vol. 31, No. 2, pp 322-329, 1994.

[6] Rinoie K, Fujita T, Iwasaki A and Fujieda H. Experimental studies of a 70-degree delta wing with vortex flaps. *Journal of Aircraft*, Vol. 34, No. 5, pp 600-605, 1997.

[7] Rinoie K. Studies of vortex flaps for different sweepback angle delta wings. *Aeronautical Journal*, Vol.101, No.1009, pp 409-416, 1997.

[8] Rinoie K. Experiments of a 60-degree delta wing with rounded leading-edge vortex flaps. *Journal of Aircraft*, Vol.37, No.1, pp 37-44, 2000.

[9] Rinoie K. Experiments on a 60° delta wing with vortex flaps and vortex plates. *Aeronautical Journal*, Vol. 97, No. 961, pp 33-38, 1993.

[10] Rinoie K. Low speed aerodynamic characteristics of 60° rounded leading-edge delta wing with vortex flaps: Part 1. 457.2mm span delta wing. College of Aeronautics Rep. No.9611, Cranfield Univ., Bedford, UK, 1996.

[11] Rinoie K, Fujita T, Iwasaki A and Fujieda H. Studies on the optimum flap deflection angle of vortex flaps. 19th Congress ICAS, Anaheim, CA, ICAS-94-4.5.4, pp 1660-1667, 1994.

[12] Rinoie K, Yamagata K and Sunada Y. Experimental studies on 50° delta wings with rounded leading-edge vortex flaps. *Journal of Japan Soc. for Aero. and Space Sci.*, Vol. 47, No. 548, pp 364-366, 1999 (in Japanese).

[13] Ellis D G and Stollery J L. The behaviour and performance of leading-edge vortex flaps. 16th Congress ICAS, Jerusalem, ICAS-88-4.5.2, pp 758-765, 1988.

Table 1 Experimental details

Λ (deg)	L.E.	fr	Cross Section	Thickness Ratio	δ_f (deg)	Re_{Cr}	Wind Tunnel (m)	Organi-sation	Ref. No.
60	Sharp	0.75	Beveled edge	3%	0-30	$6x10^5$ $9x10^5$	1x0.69 Open	CoA	9
60	Sharp	0.75	Convex Section	4.8%	0-60	$2x10^6$	2.4x1.8 Closed	CoA	5
70	Sharp	0.75	Beveled edge	3%	0-50	$1x10^6$	2x2 Closed	NAL	6
50	Sharp	0.75	Beveled edge	1.8%	0-30	$6.7x10^5$	ϕ2 Open	UTYO	7
60,70	Sharp	0.75	Flat Plate	0.5%	0, 30	$1.3x10^5$	0.6x0.6 Blow-down	UTYO	---
60	Rounded	0.75	Aerofoil Section	10%	0, 30	$8x10^5$	1x0.69 Open	CoA	10
60	Rounded	0.75	Modified Convex	4.8%	0-60	$2x10^6$ $3x10^6$	2.4x1.8 Closed	CoA	8
50	Rounded	0.75	Flat Plate	1.8%	0-30	$6.7x10^5$	ϕ2 Open	UTYO	12
60	Sharp	0.6-0.9	Beveled edge	1.8%	0, 30	$6.7x10^5$	ϕ2 Open	UTYO	---

CoA: College of Aeronautics, Cranfield University, England
NAL: National Aerospace Laboratory, Japan
UTYO: Dept. Aero. & Astro., University of Tokyo, Japan

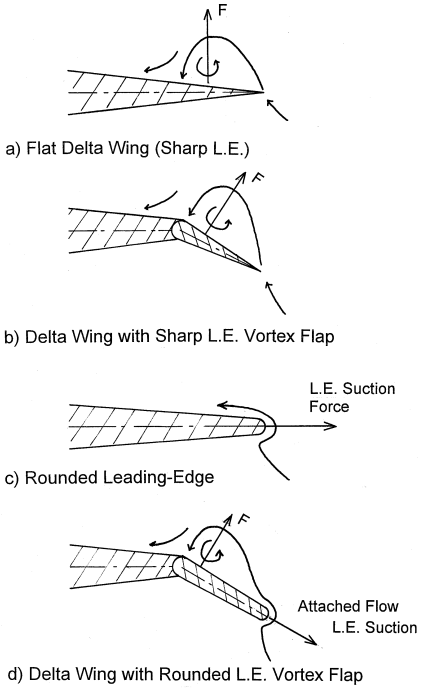

Fig.1 Concept of vortex flaps & rounded L.E. [8]

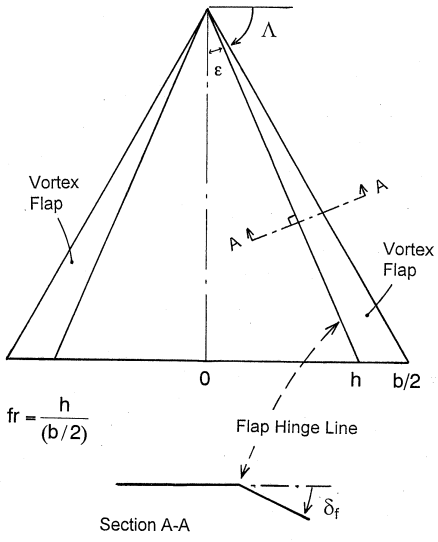

Fig.2 Delta wing with tapered vortex flaps

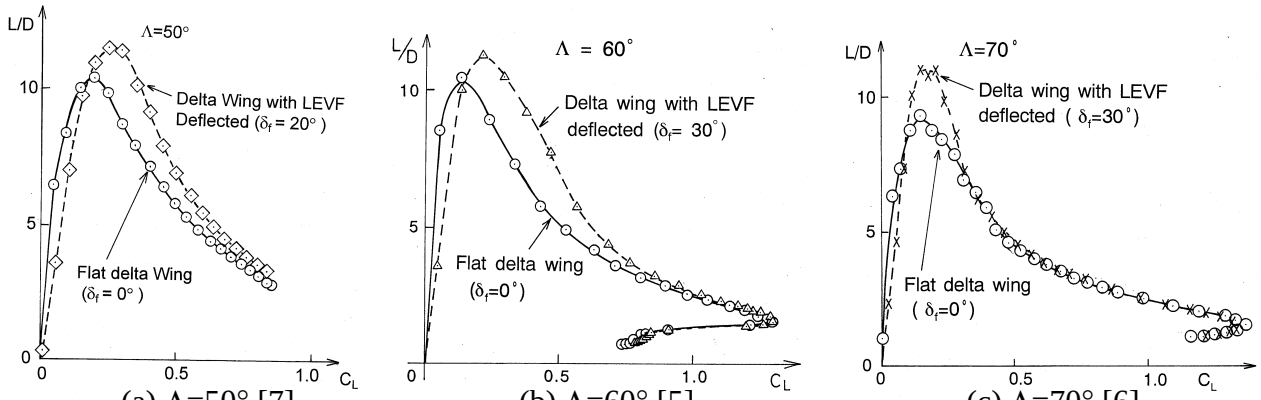

(a) Λ=50° [7] (b) Λ=60° [5] (c) Λ=70° [6]

Fig.3 *L/D* vs. C_L for sharp L.E. wing

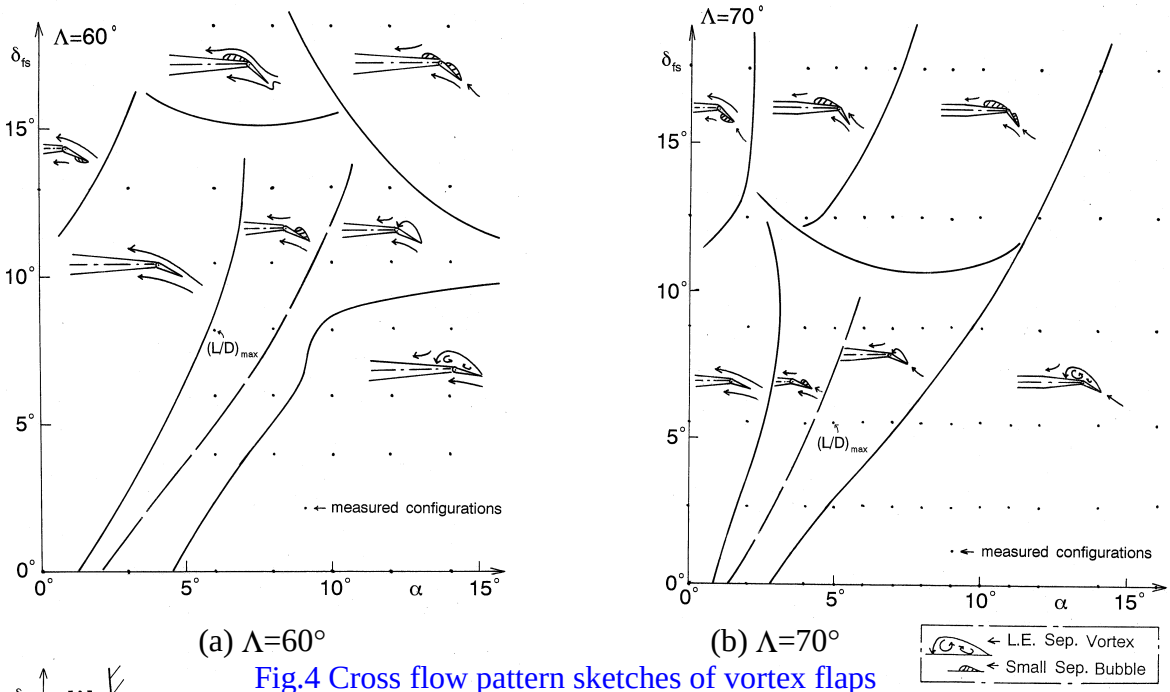

(a) Λ=60° (b) Λ=70°

Fig.4 Cross flow pattern sketches of vortex flaps

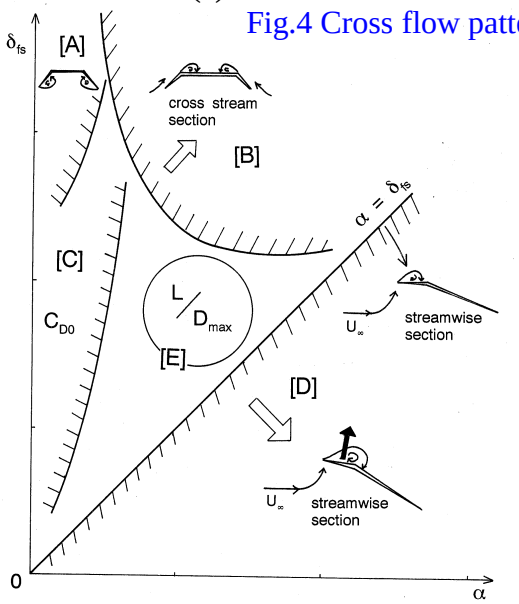

Fig.5 Schematic diagram for optimum flap defection angle

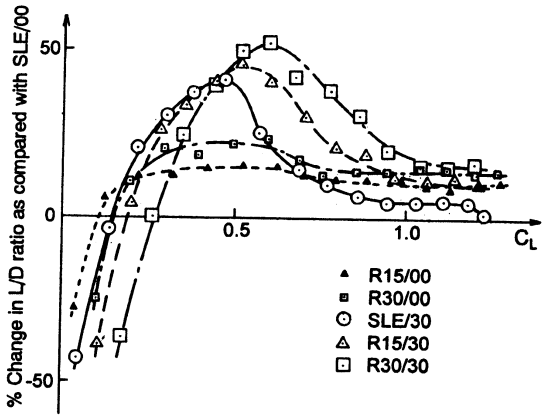

Fig.6 Benefit of rounded L.E. for 60° delta wing [8]

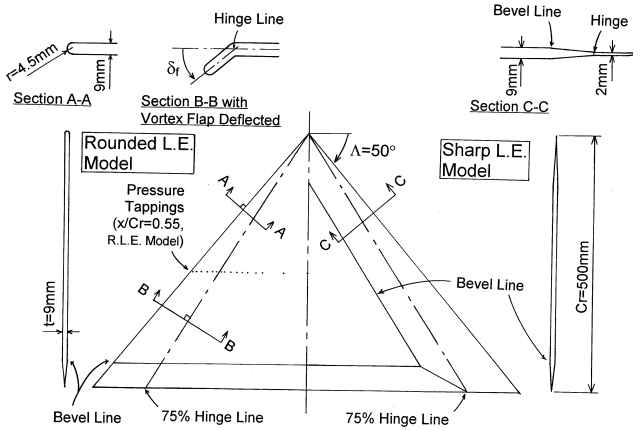

Fig.7 50° delta wing model with sharp and rounded L.E. [12]

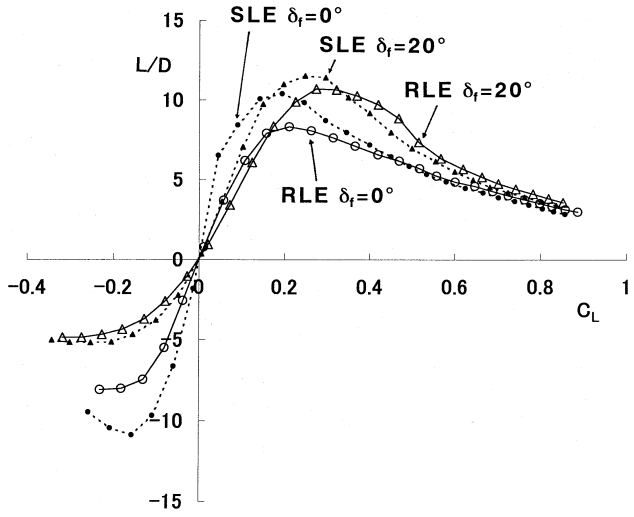

Fig.8 *L/D* vs. C_L for sharp L.E. 50° delta wing [12]

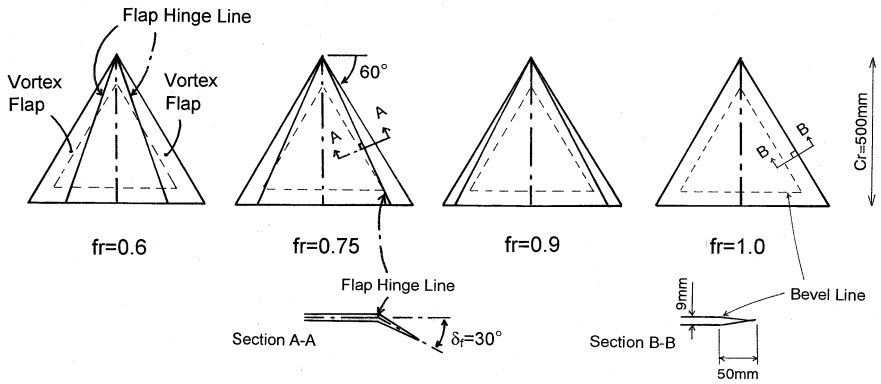

Fig.9 60° delta wing model with different *fr*

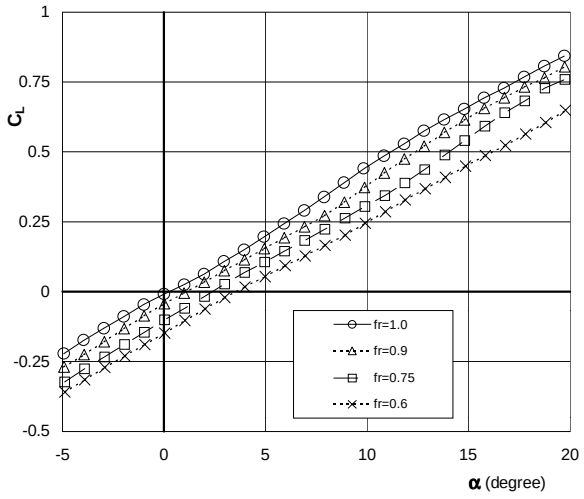

Fig.10 C_L vs. α for different *fr*

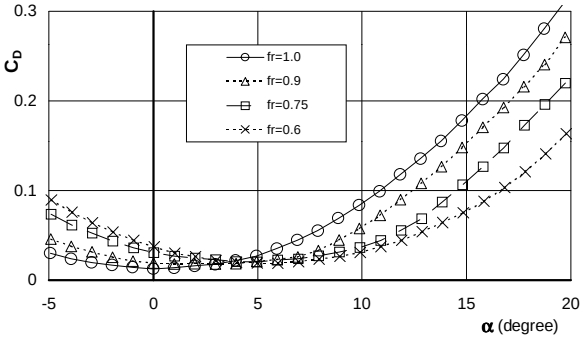

Fig.11 C_D vs. α for different *fr*

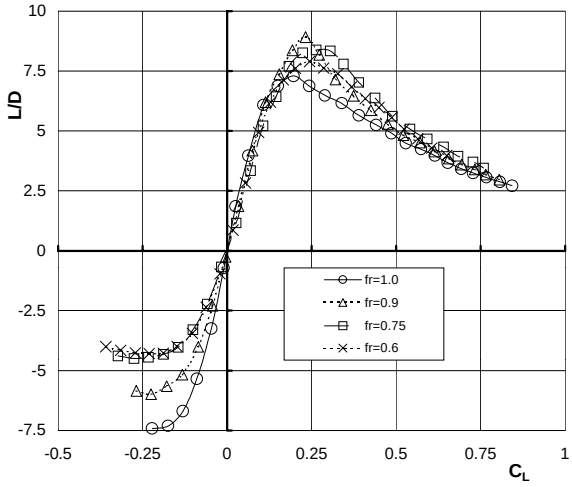

Fig.12 *L/D* vs. C_L for different *fr*

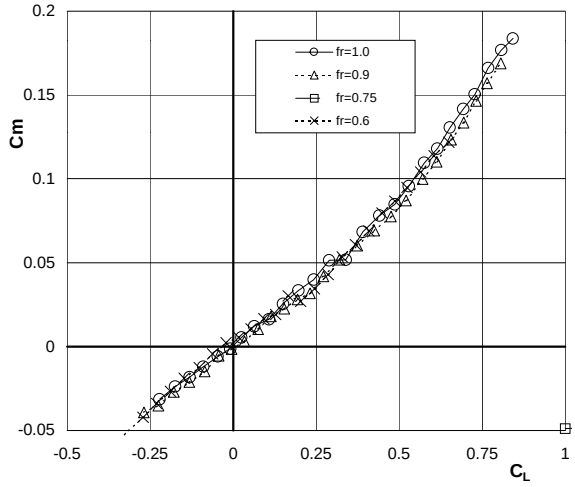

Fig.13 C_m vs. C_L for different *fr*

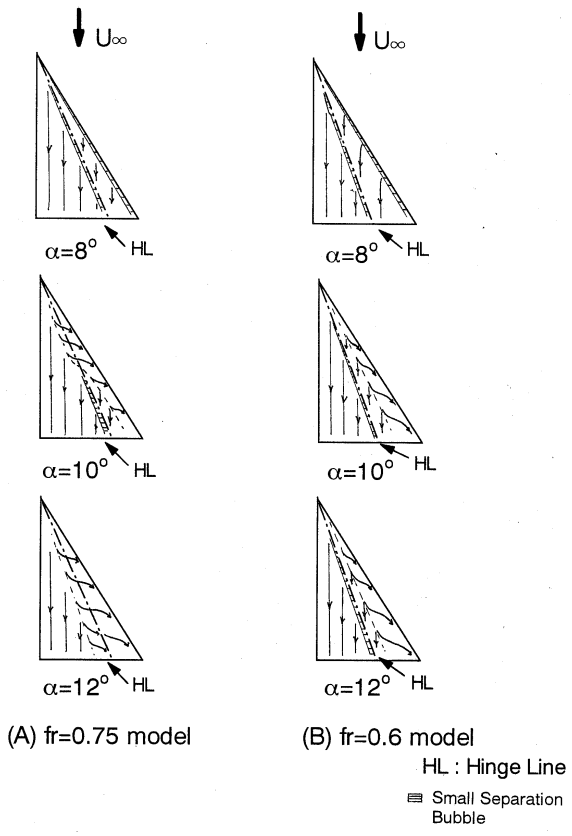

Fig.14 Surface oil flow patterns at *fr*=0.75 and 0.6

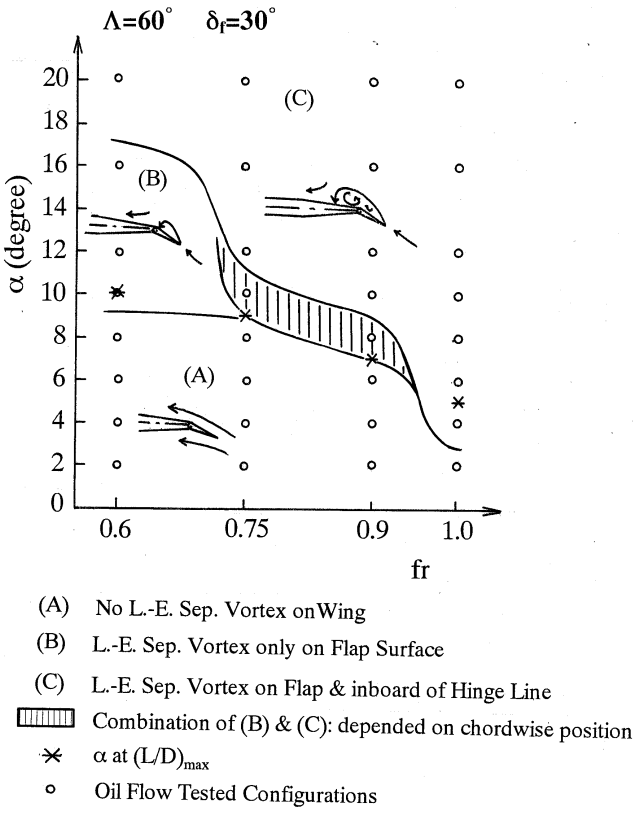

Fig.15 Cross flow patterns for different *fr*